Linear thermal expansivity (1–300 K), specific heat (1–108 K), and electrical resistivity of the icosahedral quasicrystal i-$Al_{61.4}Cu_{25.4}Fe_{13.2}$

C. A. Swenson,* T. A. Lograsso, A. R. Ross, and N. E. Anderson, Jr.
Ames Laboratory, Iowa State University, Ames, Iowa 50011

(Received 27 June 2002; revised manuscript received 3 September 2002; published 18 November 2002)

Linear thermal expansivity (α, 1–300 K), heat capacity (C_p, 1–108 K), and electrical resistivity (ρ, 1–300 K) measurements are reported for single grain i-$Al_{61.4}Cu_{25.4}Fe_{13.2}$ quasicrystals as a function of sample processing. While $\rho(T)$ is sensitive to sample treatment, both C_p and α are relatively insensitive (to a few percent) except at the lowest temperatures (below 4 K), where an inverse correlation between ρ and the electronic C_p coefficient γ appears to exist. Dispersion effects (deviations from Debye-like behavior) in both C_p and the lattice Grüneisen parameter Γ are large and comparable with those for single grain i-$Al_{71}Pd_{21}Mn_{08}$ quasicrystal and its $Al_{72}Pd_{25}Mn_{03}$ approximant [Phys. Rev. B **65**, 184206 (2002)]. Since the 0-K Debye temperature [$\Theta_0 = 536(2)$ K] is in reasonable agreement with that from 4-K elastic constants [548(8) K], a previous postulate for AlPdMn that these large dispersion effects are associated with high dispersion lattice modes in off-symmetry directions also appears to apply to i-Al-Cu-Fe. A comparison with other C_p data suggests that the major effects of sample treatment (and composition) are reflected, with a few exceptions, in the values of γ, with remarkably similar lattice contributions.

DOI: 10.1103/PhysRevB.66.184206 PACS number(s): 61.44.Br, 62.20.Dc, 65.40.Ba, 65.40.De

I. INTRODUCTION

The earliest quasicrystals were reported by Schectman *et al.*,[1] who discovered the unusual properties of rapidly solidified binary alloys of Al and Mn, Cr and Fe. The characteristic property of quasicrystals is the existence of long-range atomic order without the periodicity which is associated with crystalline symmetry. Although these first quasicrystals were metastable, and reverted to crystalline materials upon annealing, other families of quasicrystals subsequently were discovered which are single phase and stable on annealing.[2] One of the earliest of these was the icosahedral (i-) quasicrystal i-$Al_{65}Cu_{20}Fe_{15}$ which is formed after quenching the liquid alloy to room temperature.[3] Calvayrac *et al.*[4] summarized subsequent work with these alloys, and, using x-ray-diffraction pattern measurements, report that, while quenched i-$Al_{65}Cu_{20}Fe_{15}$ becomes two phase after annealing at 800 °C, the i-$Al_{63}Cu_{25}Fe_{12}$ quasicrystal is single phase, with properties which improve upon annealing.

The composition of the quasicrystal typically is written as for an alloy,[5] since, as above, quasicrystal stoichiometry may extend over a range of compositions. For Al-Cu-Fe, the 1200 °C initial molten alloy is quenched rapidly to room temperature and then is heat treated to obtain a single phase quasicrystalline state which is stable for some stoichiometries (no phase change on cooling after heat treatment) or, more often, metastable (quenched in after heat treatment, with a multiphase mixture occuring upon slow cooling). This complex Al-Cu-Fe high-temperature quasicrystal phase diagram has been studied extensively.[6–11]

The temperature-dependent physical properties of quasicrystals differ from those of normal crystalline or amorphous materials in a number of ways. Quasicrystals, like amorphous solids, are elastically isotropic, with elastic properties described completely by single longitudinal v_L and doubly degenerate transverse v_T sound velocities.[12] The low-temperature heat capacity C_p has a contribution which is linear in T and, in magnitude, is similar to, but usually somewhat smaller than, that for a metal. Quasicrystal electrical resistivities, however, often increase with decreasing T and in magnitude resemble those for semimetals.[13] The interpretation of these results in terms of a pseudogap in the density of states (DOS) at the Fermi level is supported by optical reflectivity,[14] photoemission,[15] and tunneling experiments.[15–18] Tunneling data[18] clearly show a zero-bias anomaly (ZBA) in the pseudogap which is not understood.

A number of papers have reported the effects of annealing and sample composition on Al-Cu-Fe temperature-dependent resistivities,[19–27] magnetoresistivity,[19,22,24] magnetic susceptibility,[19,20] Hall effect,[19,21,25,26] thermoelectric power,[21,25,26] and thermal conductivity.[26,27] These reports show that significant *qualitative* differences exist in a number of these properties between the compositions i-$Al_{63}Cu_{25}Fe_{12}$ and i-$Al_{62}Cu_{25.5}Fe_{12.5}$ [(25,12) and (25.5,12.5)].[20,22,24–27] Because of this potentially extreme sensitivity to small composition differences, compositions will be stated when comparing various results. Stated compositions generally are those for the initially prepared melt alloy, with little change expected on quenching.

C_p data have been published for Al-Cu-Fe samples with a range of compositions. Klein *et al.*[20] give results for a single phase (25,12) sample for which subsequent data have been obtained.[24,28,29] Wang and collaborators[30,31] measured C_p for as-cast and annealed samples of i-Al-Li-Cu (1–7 K) and (25.5,12.5) i-Al-Cu-Fe (1–3 K), and found that, while annealing has little effect for Al-Li-Cu, C_p is reduced significantly for Al-Cu-Fe. Pierce *et al.*[25] show 1–4.5 K results for several Al-Cu-Fe samples [i-(26.5,11), (rhombohedral) r-(26.5,11), i-(24.5,13), and i-(24.5,12) from Ref. 21, where C_p results for r-(24.5,12) are given also]. Lasjaunias and his collaborators[28,29] give C_p results for the common i-(25,12) sample of Ref. 20 (1.5–12 K) and Ref. 24 (0.1–4

K) [designated as (25,12)-(a)], for a second (better quality) sample from the same original material [(25,12)-(b)] (0.1–7 K and 4–40 K in separate calorimeters), and for a (25.5,12.5) sample (0.1–7 K).

A direct relationship exists between low-temperature $C_p(T)$ data and low-temperature sound velocities as determined both acoustically and from the limiting low-energy slopes of inelastic neutron scattering (INS) acoustic dispersion relations.[32] Vanderwal *et al.*[33] obtained the longitudinal and transverse sound velocities (elastic constants) for *i*-(24.5,12) from Brillioun scattering data. Tanaka *et al.*[34] used resonant ultrasound spectroscopy (RUS) to obtain the temperature-dependent elastic constants for *i*-(20,15) (and Al-Pd-Mn and Al-Cu-Fe-Ru) from 4 K to 800 °C. RUS techniques[35] are particularly useful for measurements on quasicrystals since resonances for many different directions in a sample are used to determine the characteristic sound velocities (elastic constants), and can provide an excellent confirmation of elastic isotropy.[36] Bert *et al.*,[37] in an investigation of tunneling states in *i*-(25,12), give a 4-K v_T which is somewhat smaller than that from the other investigations. This sample initially was characterized in a neutron-diffraction study.[38]

Neutron-scattering data not only give sound velocities, but also can be used to calculate $C_v(T)$. INS studies for major symmetry directions of single grain *i*-(25,12) by Quilichini and co-workers[39–41] are consistent with elastic isotropy and show linear energy vs wave-number relations (no dispersion) at energies from 1.4 to 2.5 THz (67 to 120 K). These results are summarized in a review paper,[42] where 400 °C sound velocities are given which are consistent with ultrasonic data. Brand and co-workers[43,44] discuss problems with the generalized vibrational density of states (GVDOS) which follows from the INS measurements, and describe results from a time-of-flight (TOF) inelastic neutron-scattering experiment using *i*-(25.5,12.5) samples which (i) have natural isotopic abundances, or have been prepared with isotopically pure (ii) ^{65}Cu or (iii) ^{57}Fe. Their resulting neutron weighted GVDOS is used to calculate the temperature dependence of C_p and which is in agreement with the results of Lasjaunias *et al.* to 7 K on the same sample which show unusual dispersion behavior.[29] They conclude that a discrepancy between these directly measured and calculated C_p's and those calculated from sound velocities probably is due to ''nonacoustic vibrational elementary excitations.''[44] This conclusion is associated with the observation by Lasjaunias and his collaborators that the temperature dependence of their C_p's at low temperature are not consistent with Debye-like behavior.[28,29]

A previous paper[32] describes data similar to the present for *i*-$Al_{71}Pd_{21}Mn_{08}$ and its ξ' approximant. While the existence of large single grain samples of Al-Pd-Mn quasicrystals[45] makes them attractive for both linear thermal expansivity (α) and C_p studies, the formation of a spin glass on cooling below 11 K (associated with a small fraction of the Mn^+) masks the quasicrystal properties. The Al-Pd-Mn results gave precise quasicrystal (and approximant) α data from 1 to 300 K, with complementary C_p, electrical resistivity, magnetic susceptibility, and elastic constant data to characterize the samples.

The C_p and α data for AlPdMn suggest large dispersion (non-Debye behavior) effects below 4 K which are inconsistent with the much higher energy dispersion effects from inelastic neutron-scattering results.[42] The neutron-scattering data are for major symmetry directions (near strong Bragg peaks),[42] since neutron-scattering intensity is highly dependent on the strength of the nearby Bragg reflections. The RUS experiments[34,32] show that low-frequency acoustic waves (isotropic longitudinal, degenerate transverse) exist for all directions in the crystal. If a standard lattice model is assumed, the zone boundaries which determine the energy gaps in the dispersion relations depend inversely on the magnitude of the lattice repeat distances. These repeat distances are small for the major symmentry directions, hence dispersion effects occur at relatively large energies.[42] The repeat distances are highly variable and much greater away from the major symmentry directions, so it is reasonable to postulate that the generally much smaller zone boundaries will result in much smaller maximum energies for the phonons in these directions.[46] Most of the phonons in these materials will be associated with these off-major symmetry directions, so the lattice GVDOS will show large low-energy dispersion effects with an initial (sound velocity determined) Debye-like form.[32] This will result in the excessively large dispersion effects in $C_v(T)$. While this low-energy behavior cannot be determined in INS experiments, the agreement between the $C_v(T)$'s of Lasjaunias *et al.*[29] and those calculated from the neutron weighted GVDOS of Ref. 44 undoubtedly includes these effects. These off-symmetry vibrations are acoustic and are responsible for the extremely rapid increase (with respect to a Debye solid) of the GVDOS with increasing temperature.

The objectives of the present experiment were twofold. The first was to ascertain whether or not the large dispersion effects in C_p (and a very different temperature dependence for α at low temperature) for *i*-Al-Pd-Mn and its ξ' approximant also exist in *i*-Al-Cu-Fe. The second was to determine the effect of sample processing and treatment on C_p and α. The present data for single grain samples of *i*-$Al_{61.4}Cu_{25.4}Fe_{13.2}$ show behavior very similar to that for Al-Pd-Mn, and a relative insensitivity to sample state. The large, unique, dispersion effects for both *i*-Al-Pd-Mn and *i*-Al-Cu-Fe suggest a universal characteristic of quasicrystals which is associated with their unique structure.

II. EXPERIMENTAL DETAILS

The single grain samples studied in the present paper were grown by a liquid-assisted grain growth technique described in detail elsewhere.[47–49] Appropriate quantities of aluminum, copper, and iron (99.99% purity, metals basis) were arc melted into buttons of nominal composition $Al_{62}Cu_{25.5}Fe_{12.5}$. The buttons were chill cast into cylindrical ingots which were roughly 25-mm diameter and 70-mm length. The ingots were placed in an alumina crucible, sealed in quartz under ultrapure argon and subjected to multiple heat treatments at 835 °C. Following heat treatment, a

single-crystal grain, exhibiting fivefold facets and approximately 0.5 cm^3 in size, was harvested from the ingot and represents the as-grown condition. In this condition, the crystal is porous (up to 10%) and contains a small fraction of second phase.[49]

This as-grown crystal was subjected to two further treatments. The first used hot isostatic pressing (HIP, argon gas) at 800 °C and 315 MPa for 4 h (pressurizing at temperature), followed by a furnace cool (uncontrolled, furnace power off) as the pressure was released, to reduce the porosity to 1% or better. Subsequently, the sample was sealed in a fused quartz ampoule with a partial pressure of argon and was annealed at 800 °C for 6 h and furnace cooled to eliminate the second phase.[48]

C_p and α data were taken at various stages for two samples from the same boule which were treated using different variations of the HIP cycle. The first sample was measured in the as-grown (initial) state (sample 1), then underwent HIP as above and a second (sample 2) set of data taken. Finally, the sample was annealed for a third (sample 3) set of data. The second sample underwent HIP as above, but the pressure was released isothermally at 800 °C and the sample annealed *in situ* at this temperature for another 4 h, after which it was furnace cooled and a fourth (4) set of data taken. A final (5) set of data was taken after the sample was given a standard anneal. To summarize for the following presentation of the data, 1, 2, and 3 refer to subsequent treatments of the same physical sample, 4 and 5 to treatments of a second physical sample from the same boule. A subsequent ICP (inductively coupled plasma atomic emission spectrometry) analysis of the sample material gave the composition $Al_{61.40}Cu_{25.44}Fe_{13.23}$, which will be rounded off in the following as $Al_{61.4}Cu_{25.4}Fe_{13.2}$, or (25.4,13.2).

The hardware and procedures used for the resistivity, C_p, and α measurements are identical with those described in an earlier paper.[32] Two resistivity samples (approximately $1\times1\times5$ mm) were measured, one of which was included in each of the above sample procedures. The precision of these data was better than 1%, with a systematic uncertainty of 5% due to dimensional uncertainties. The C_p and α samples were irregularly shaped, with a flat base and approximately 12 mm in height to accommodate the dilatometer. The masses of the first samples (1, 2, 3) were approximately 3.5 g, while those for second sample (4, 5) were of the order of 1.9 g. The C_p data were taken from 1 to 108 K using a standard tray-type isothermal calorimeter,[50] while the 1–300 K α data used a differential capacitance dilatometer which was calibrated with high-purity copper.[51]

III. EXPERIMENTAL RESULTS

A. Resistivities

The temperature dependences of the resistivities (ρ) for the various sample treatments are shown in Fig. 1. Sample 1 (○) is for the large, porous, single grain starting material, and probably is overestimated since no correction was made for the porosity.[49] Sample 2 (□) is for the same sample after undergoing HIP; $\rho(T)$ has increased significantly, presumably due to the generation of phasons (strains) in the HIP process. Sample 3 (△), sample 2 after annealing, shows a substantial decrease to a $\rho(T)$ relation which is essentially the same (due to dimensional uncertainties) as that for sample 4 (for the second physical sample after a combined HIP and annealing). Because of this correspondence, this resistivity sample was not included in the subsequent 5 heat treatment, after which additional C_p and α data were taken.

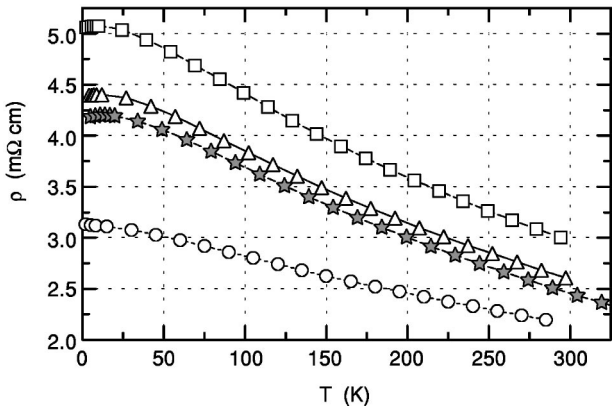

FIG. 1. The temperature dependence of the resistivities for samples with various heat treatments: (○) 1, (□) 2, (△) 3, (⋆) 4, (◇) 5 (not shown). See the text for details.

The present sample 3 (25.4,13.2) resistivity results are very similar to published $\rho(T)$ results for (25,12) compositions which are in substantial agreement, with $\rho=4.7(3)$ and 2.7(2) mΩ cm at 4 and 300 K, respectively,[19,20,22–26] and are appreciably smaller than those published for similar [nominal (25.5,12.5)] compositions. The largest published 4 K values of ρ appear to be for (25,12.5) (11 mΩ cm);[20,23,24] the values for (25.5,12.5) [7.5(15) mΩ cm] are somewhat smaller.[20,23,24,26] These differences between the (25,12) and (25–25.5,12.5) compositions have been interpreted to indicate an extreme sensitivity to composition and proximity to a metal-insulator transition.[20,24] A similar qualitative sensitivity to composition is found in thermoelectric power, thermal conductivity, and Hall-effect data.[25–27]

B. Representation of C_p and α data

The bases for the presentation of the *i*-$Al_{63}Cu_{25}Fe_{12}$ C_p and α data are given in a previous paper,[32] and are summarized in the following. The basic equations used to represent low-temperature data are

$$C_p/T=\sum_{n=0}^{N} C_{2n+1}T^{2n}, \tag{1a}$$

$$\alpha/T=\sum_{n=0}^{N} A_{2n+1}T^{2n}. \tag{1b}$$

The lead parameters, C_1 and A_1, generally are ascribed to electronic contributions, with $C_1=\gamma$, the electronic specific-heat coefficient, although, for amorphous solids, a linear term also has been associated with a distribution of tunneling states.[52] In most instances, higher-order terms are associated

with lattice properties (C_p^{lat}), with the characteristic $T=0$ Debye temperature Θ_0 given by[53]

$$\Theta_0^3=[(12\pi^4/5)rR/C_3]$$
$$=[1.944\times10^6 r(\text{mJ/g mol K})/C_3]\ \text{K}^3, \quad (2)$$

where R and r are the gas constant and the number of atoms per unit cell, respectively. This equation has no significance for tunneling systems, where the ''lattice'' contribution C_3 often is appreciably greater than would be calculated for a Debye solid [see Eqs. (3) below].[52]

Θ_0 also can be calculated from an average 0 K sound velocity as[53]

$$\Theta_0^3=(h/k_B)^3(3rN_0/4\pi V_m)(1/\langle 1/v^3\rangle) \quad (3a)$$

which for an isotropic quasicrystal (two sound velocities; v_L and a twofold degenerate v_T) is

$$=(h/k_B)^3(3rN_0/4\pi V_m)v_T^3\{3/[2+(v_T/v_L)^3]\} \quad (3b)$$

$$=(2.5142\times10^{-3})^3(r/V_m)v_T^3\{3/[2+(v_T/v_L)^3]\}, \quad (3c)$$

where h is Planck's constant, k_B the Boltzmann constant, N_0 Avagadro's number (/g mol), V_m the molar volume [m^3/(g mol)], r the number of atoms in a unit cell, and the sound velocities are in m/sec. These velocities are related to the elastic constants as $C_T=C_{44}=\varrho v_T^2$, and $C_L=C_{11}=\varrho v_L^2$. Note that the density ϱ enters into Eqs. (3) only through the definition of the molar volume. At ''high'' temperatures (>30 K), power series similar to Eqs. (1) are used, with T^n rather than T^{2n}; the parameters for these series have no physical significance.

At low temperatures (below $\Theta_0/10$), the extremely strong temperature-dependence of C_p presents difficulties in the display of data for any range of temperatures. Since the Debye function approximates this temperature dependence, it is reasonable to use the Debye function as the basis for displaying C_p results; one procedure for accomplishing this is to relate experimental lattice $C_v(T)$'s [$C_v^{lat}=C_v(T)-\gamma T$] (see Ref. 54) directly to the Debye function using equivalent Debye Θ's.[55] For a C_v^{lat} datum at T, $\Theta(T)$ is the Debye temperature which, when used in the Debye relation for C_v (C_{Debye}, Ref. 53), will give the same C_v at that temperature,

$$C_v^{lat}(T)=C_v(T)-\gamma T=C_{Debye}[\Theta(T)/T]. \quad (4)$$

A plot of $\Theta(T)$ vs T shows deviations of the data from the Debye function, or the effects of dispersion; a decreasing Θ represents an increasing positive deviation of C_v from Debye behavior. When comparing materials with significantly different Θ_0's, a normalized plot of $\Theta(T)/\Theta_0$ vs T/Θ_0 will display clearly differences in the shapes of the $C_v(T)$ relations.

The volume thermal expansivity ($\beta=3\alpha$ for an isotropic solid) is related directly to $C_v(T)$ by the Grüneisen relation:[55,56]

$$\beta=3\alpha=\Gamma(C_v/B_TV)=\Gamma(C_p/B_SV). \quad (5a)$$

where B_T and B_S are the isothermal and adiabatic bulk moduli, V is the molar volume, Γ is the dimensionless Grüneisen parameter, and $C_p/C_v=B_S/B_T$.[54] If independent (separable) contributions (electronic, lattice, magnetic, etc.) to the thermodynamics of an isotropic solid can be identified, each contribution will have a C_{vi} and a Γ_i associated with it, and the individual thermal expansivities will be additive to give for an isotropic material,

$$\beta=\sum\ \beta_i=3\sum\ \alpha_i=\sum\ \Gamma_iC_{vi}/B_TV. \quad (5b)$$

In this model, the Γ_i's are given by

$$\Gamma_i=3B_TV(\alpha_i/C_{vi})=-d\ln\Phi_i/d\ln V, \quad (6)$$

where the characteristic energy Φ_i may be Θ_0 for the lattice, the Fermi energy for free electrons, the Curie temperature for a magnetic system, etc. Values of Γ typically range from ±1 to ±4, although Γ will have much larger magnitudes when Φ has a large volume sensitivity, such as that associated with tunneling.[52,56] The lattice Γ, Γ^{lat}, generally has a temperature dependence similar to that of $\Theta(T)$, since the lattice modes which are excited with increasing T may have significantly different volume dependences. By analogy with $\Theta(T)$, Γ_0^{lat} is the limiting, $T=0$ value of $\Gamma^{lat}(T)$, and, at high T, Γ^{lat} approaches a constant value Γ_∞^{lat}. Since $\Gamma_0^{lat}=-d\ln\Theta_0/d\ln V$, Θ_0^{lat} also can be calculated from the volume (pressure) dependence of the sound velocities [Eqs. (3)].

C. C_p and α data

The present C_p and α data plotted as a function of temperature in Fig. 2 have been normalized by T to reduce the temperature dependence. Above 20 K, the major difference between the five sets of C_p data [$+3(1)\%$] occurs for the as-received [(○)1] sample at the highest temperatures, with the HIP sample [(□)2] showing a small [$-1.5(5)\%$] systematic deviation (not evident) between 20 and 70 K. The agreement above 20 K between the C_p's for the final treatments of the original (3) and the second (5) samples suggests that these should be accepted as characteristic of a ''pure'' sample. The fit to sample 3 [barely visible as a solid line in Fig. 2(a)] is an excellent representation for these data above 20 K. The situation for the α data [where the fit to the sample 3 data is given by the solid line through the (△) in Fig. 2(b)] is not as clearcut, with the four other sets of data differing systematically from this line by $-3(1)\%$ above 60 K.

The C_p/T vs T^2 representations [see Eq. (1a)] in Figs. 3 and 4 show that the general agreement between the various C_p data extends down to 1 K. The lower temperature data in Fig. 4(a) [below 4 K ($T^2<16\ \text{K}^2$)] tend to be high for the as-received sample 1 (○), and to be somewhat low for the 2 HIP sample (□); this correlates inversely with the resistivities in Fig. 1. The solid lines (—-) represent fits of Eq. (1a) (with nine parameters) to the sample 3 C_p data from 1 to 35 K, with $\gamma=0.285(1)$ mJ/mol K^2 and $\Theta_0=536(2)$ K. A three-parameter fit to the sample 3 data from 1 to 10 K gives values of γ and Θ_0 within these uncertainty limits. Similar

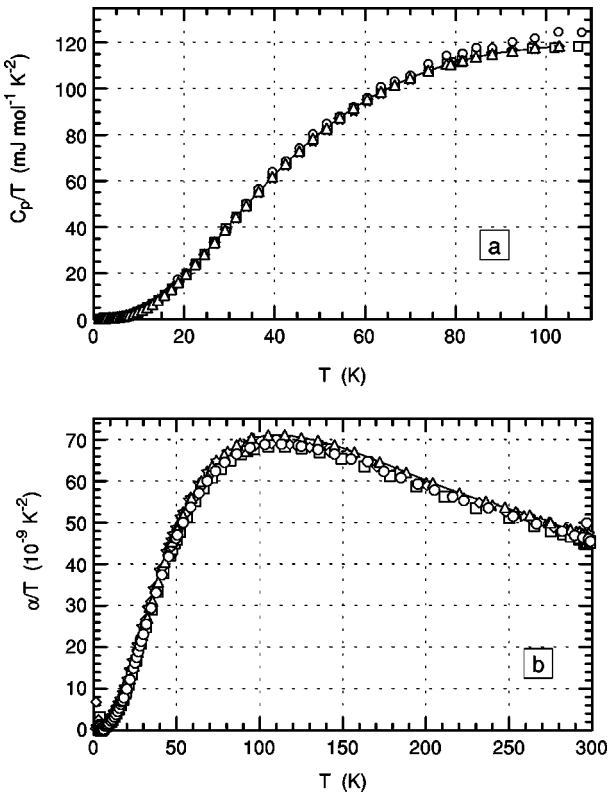

FIG. 2. C_p/T (a) and α/T (b) vs T for the present data. The symbols indicate various heat treatments, as in Fig. 1: (○) 1, (□) 2, and (△) 3 for the original, (⋆) 4 and (◇) 5 for the second samples. The solid lines (——-) are from fits to the sample 3 data. See the text for details.

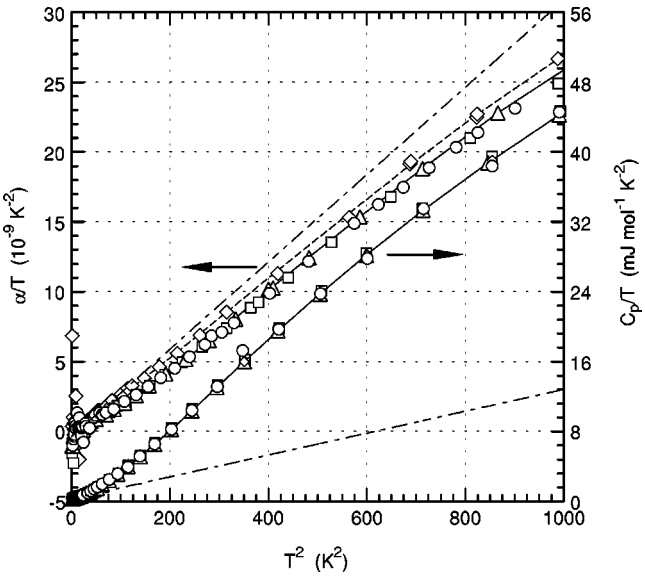

FIG. 3. α/T (left) and C_p/T (right) vs T^2, with markers as in Fig. 2, without 4 (⋆). (—) and (– – –) are fits to the sample 3 and sample 5 data, respectively, (– — –) are dispersionless (Debye) extrapolations from 0 K using the two lead parameters in Eqs. (1). Note the different origins for α and C_p.

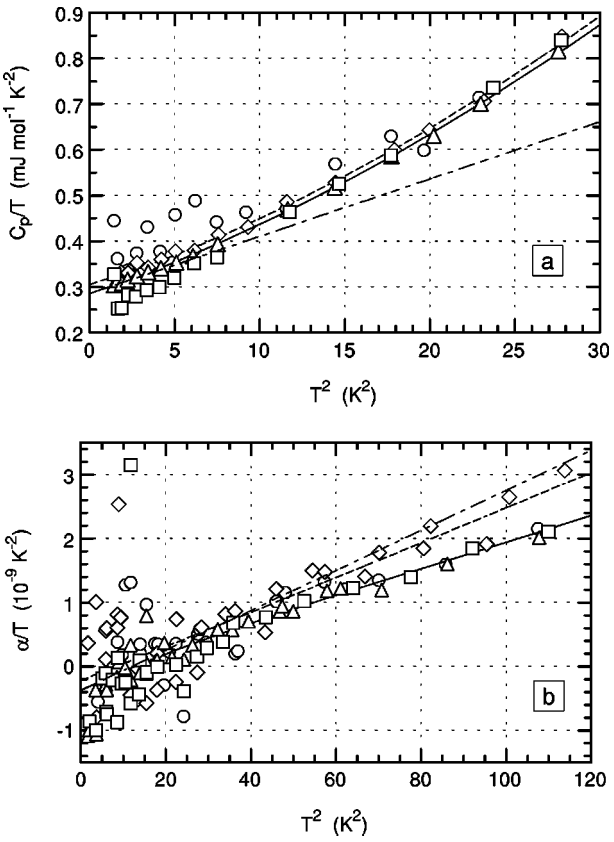

FIG. 4. C_p/T (a) and α/T (b) vs T^2 for the lower-temperature region of the data plotted in Fig. 3. Note the different T^2 axes for the two plots.

fits to the sample 5 data suggest a slight upturn below 3 K [not evident in Fig. 4(a)], with a fit of Eq. (1a) to the data from 3 to 35 K (– – –) giving $\gamma = 0.296(1)$ mJ/mol K^2 and $\Theta_0 = 541(1)$ K. The differences are small, and within the experimental scatter at the lowest temperatures. The consistency in the values of γ and Θ_0 for fits of Eq. (1a) for very different maximum temperatures (1–10, 1–35 K) suggests that it is unlikely that the large dispersion effects are associated with a low-lying optical mode.[44]

The first part of Table I summarizes the results of fits of Eq. (1a) to the various data; the uncertainties stated for γ (C_1) and Θ_0 ($\sim C_3^{-1/3}$) for a stated maximum fit range reflect the spread of parameter values for the several fits (varied maximum temperatures, number of parameters required) involved. A dependence of the results on the minimum temperature indicates a possible excess curvature at low temperature, as for sample 5 above. In general, the smaller γ's are associated with smaller Θ_0's [a larger slope in Fig. 4(a)], since the lattice C_p's are very similar above 3 K.

Because of its internal consistency, the 1–35 K representation of sample 3 has been chosen, somewhat arbitrarily, as the standard for the current presentation. The two lead sample 3 parameters in Eq. (1a) [C_1 (γ) and C_3 ($\sim\Theta_0^{-3}$)] were used to generate the (– — –) lines in Figs. 3 and 4(a) which represent C_p/T vs T^2 for a Debye solid. The differences between these lines and the data reflect the extremely dispersive, or non-Debye, nature of the lattice excitations in these quasicrystals.

TABLE I. A summary of C_p-related parameters from the present experiments and from various references. γ_{norm} has been determined from a normalization to the present higher T data for sample 3. Where Θ_0 and γ are (–), curvature of the low-temperature C_p/T vs T^2 data precluded the direct determination of these quantities. See the text for details.

Θ_0 c (K)	γ (mJ/mol K^2)	γ_{norm}	Sample	Comments
560(35)	0.32(2)	–	i-(25.5,13.2)	present 1, 3–30 K
480(3)	0.227	–	i-(25.5,13.2)	present 2, 1.2–35 K
503(4)	0.253	–	i-(25.5,13.2)	present 2, 3.4–35 K
536(2)	0.285	0.285	i-(25.5,13.2)	present 3, 1–35 K
530(6)	0.280	–	i-(25.5,13.2)	present 3, 4–35 K
573(4)	0.27(2)	–	i-(25.5,13.2)	present 4, 1.4–30 K
631(5)	0.317	–	i-(25.5,13.2)	present 4, 3–30 K
554(1)	0.305	–	i-(25.5,13.2)	present 5, 1–30 K
541(2)	0.296	–	i-(25.5,13.2)	present 5, 3–30 K
370	0.30	–	i-(25,12)[-(a)]	Klein (Refs. 20,24,29)
273(5)	0.33	–	i-(25.5,12.5)	as recd., Wang (Refs. 30 and 31)
350(5)	0.30	–	i-(25.5,12.5)	annealed, Wang (Refs. 30 and 31)
539	0.31	0.29	$i-$(24.5,12)	Biggs (Refs. 21 and 25)
583	0.29	–	r-(24.5,12)	Biggs (Refs. 21)
560	0.32	0.33	$i-$(26.5,11)	Pierce (Ref. 25)
555	0.25	0.25	r-(26.5,11)	Pierce (Ref. 25)
560	0.35	0.35	i-(25,12)-(b)	Lasjaunias (Ref. 29)
–	–	0.37	i-(24.5,13)	Pierce (Ref. 25)
–	–	0.41	i-(25.5,12.5)	Lasjaunias (Ref. 29)
–	–	0.40	i-(23,12)	Poon (Ref. 57)
–	–	2.12	i-(20,15)	as cast, Poon (Ref. 57)
–	–	0.77	i-(20,15)	annealed, Poon (Ref. 57)
518(5)	–	–	i-(24.5,12)	Brill. Scat. Vanderwal (Ref. 33)
529(8)	–	–	i-(20,15)	RUS: 300 K, Tanaka (Ref. 34)
548(8)			i-(20,15)	RUS: 4 K, Tanaka (Ref. 34)
501			i-(25,12)	INS: 673 K, Quilichini (Ref. 42)

The last four rows in Table I contain citations to various acoustic velocity determinations from which Θ_0^{el} can be calculated [Eqs. (3)]. Vanderwal *et al.*[33] estimated the room-temperature acoustic velocities in $i-(24.5,12)$ from Brillouin scattering spectroscopy of surface waves, from which, accepting the stated precision, $\Theta_0^{el}=518(5)$ K. Tanaka *et al.*[34] used RUS (resonant ultrasound spectroscopy[35]) data to obtain the elastic constants of i-(20,15) from 4 to 800 K, from which $\Theta_0^{el}=548(8)$ and 529(8) K at 4 and 290 K, respectively; the uncertainties are associated with estimated impurity phases in this sample. Finally, Quilichini and Janssen[42] give sound velocities from earlier 400 °C inelastic neutron-scattering data[39] from which $\Theta_0^{el}=501$ K, with no uncertainties given. The 4 K $\Theta_0^{el}=548(8)$ K from Tanaka *et al.*[34] (Table I) is in reasonable agreement with our result [536(2) K]. The difference, in part, can be associated with the smaller atomic weight of the RUS sample. Unfortunately, a lack of sufficient quality samples prevented elastic constant measurements for the present material.

Figure 5 gives the equivalent $\Theta(T)$ representation [Eq. (4)] of the lattice C_p of sample 3 ($\triangle$) for the full temperature range of the data. This relation shows graphically the large dispersion effects in this material, with a Debye solid corresponding to a horizontal line at Θ_0. $\Theta(T)$ for the i-(25,12)-(b) C_p data of Lasjaunias *et al.*[29] also are shown in Fig. 5 ($\square$); these are the only other Al-Cu-Fe data which

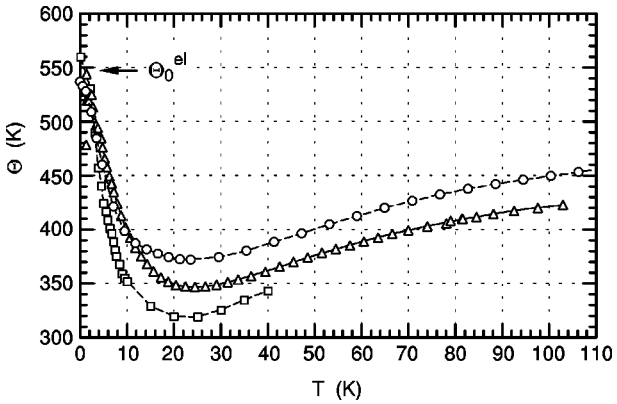

FIG. 5. Equivalent Θ's for the present (sample 3) (25.4, 13.2) Al-Cu-Fe data ($\triangle$), the (25, 12)-(b) data from Ref. 29 ($\square$), and for the Al-Pd-Mn ξ' approximant, as normalized using Θ_0 ($\bigcirc$). (Refs. 32 and 58). See the text for details.

extend to "high" temperatures, and show even greater dispersion effects than for the present data. Similar behavior was reported for the C_p's of i-$Al_{71}Pd_{21}Mn_{08}$ and its ξ' approximant, with the suggestion that a uniquely rapid onset of dispersion is a property of quasicrystals.[32] An adjusted[58] $\Theta(T)$ relation for this Al-Pd-Mn approximant (○), which should resemble closely that for the quasicrystal, also is shown in Fig. 5.

In Figs. 3 and 4(a), the α data for the various treatments of the first sample [original (○), HIP (□) and final (△)] are in good agreement, and are systematically smaller than those for the final second sample final [(◇)5], and, not shown, 4 results. In these figures, the solid lines (—-) are from a six-parameter fit (using absolute differences) of Eq. (1b) to the sample 3 α data from 1.3 to 22 K, and a nine-parameter power series (α/T vs T) fit from 22 to 300 K. The dashed (– – –) lines represent similar fits to the sample 5 data. Apparently, there are no other α results for comparison with these present data. At 293 K, $\alpha = 1.385(8) \times 10^{-5}$ K^{-1}.

The small difference between the α data for the two samples in Fig. 3 disappears at lower temperatures [Fig. 4(b)] where α becomes negative. The scatter in the low-temperature α data in Fig. 4(b) is consistent with a precision in the determination of length changes of ± 0.15 Å (1.5×10^{-9} cm) for these 1.2 cm long samples and a 0.5 K temperature change. The (– —— –) in Figs. 3 and 4(b) represent an extrapolation to higher temperatures using only the first two terms in Eq. (1b), and represent low-temperature Debye-like (Γ, Θ constant) behavior of α for a metal. In contrast with the behavior for C_p in Figs. 3 and 4(a), dispersion effects are small for the quasicrystal α's, and are negative. This implies a significant decrease of the Grüneisen parameter [Eq. (6)] with increasing temperature.

Figure 6 shows the temperature dependences of the lattice Grüneisen parameters, Γ^{lat} [Eq. (6)], for the present samples 1, 2, 3, and 5. The 4 K value of the bulk modulus,[34] $B_T = 108$ GPa, density $= 4500$ kg/m^3, and gram atomic weight $= 0.039\,59$ kg/g mol give for Eq. (6), $3B_TV = 2.85 \times 10^9$ J/g mol, which should be effectively independent of temperature for the present data. The Γ^{lat} data points in these figures were calculated from the actual α data [$\alpha^{lat} = (\alpha - A_1T)$, by analogy with Eq. (4)] and C_p's from the corresponding smooth relations. Hence the scatter in the data points in Fig. 6 reflects directly the scatter in the (lattice) α data, as in Fig. 4(b). Equation (6) was used to calculate the smooth Γ^{lat} curves from the fits to the α and C_p data for sample 3 (——) and sample 5 (– – –), respectively. The rapid decrease of γ^{lat} from a relatively large extrapolated value of $\Gamma_0^{lat} = 6.8(3)$ at 0 K to 1.69(3) above 30 K is a direct result of the very different temperature dependences of α and C_p in Figs. 3 and 4.

The expected differences in the values of Θ_0 from 300 and 4 K elastic constants can be calculated using Eq. (6), $d \ln \Theta_0 = -\Gamma^{lat} \times d \ln V$, since the volume changes are small, and Γ^{lat} essentially is constant for most of the volume change [Figs. 2(b) and 6(a)]. The integrated α data give $[V(0) - V(300)]/V = -7.80 \times 10^{-3}$ which, with $\Gamma^{lat} = 1.69$,

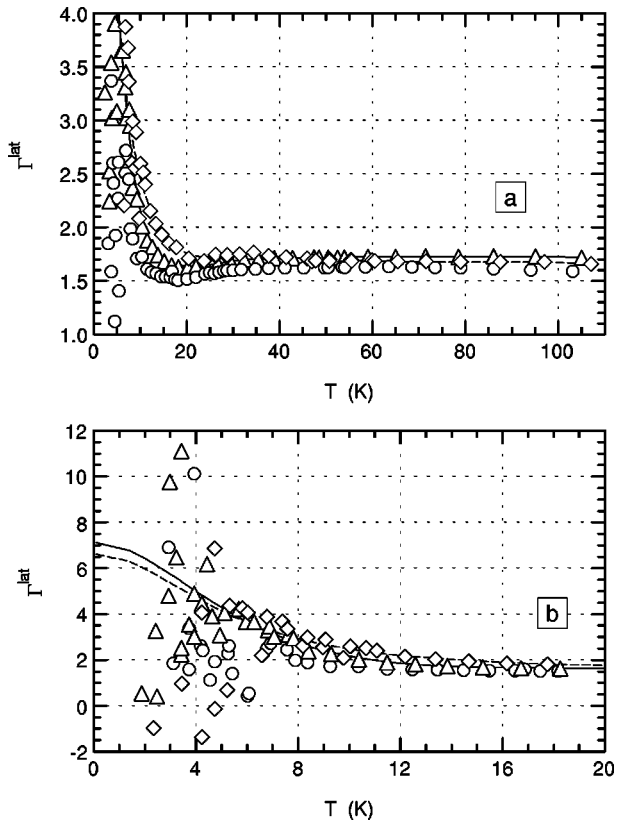

FIG. 6. Temperature dependences of the lattice Γ's [Eq. (6)]. The markers and lines are as in Figs. 3 and 4.

gives $d \ln \Theta_0 = 0.0132$, or $\Theta_0(0) - \Theta_0(300) = 7$ K. This difference compares with 19 K from the data of Tanaka *et al.*[34] in Table I. A similar discrepancy exists for Al-Pd-Mn.[32]

The linear (electronic) Grüneisen parameters, Γ^{lin} [which are obtained using the ratio A_1/C_1 in Eq. (6)], are predominantly negative, and depend on the extrapolation of the α/T plot [Fig. 4(b)] to 0 K. Their values [0.8 (sample 1), −8.5 (sample 2), −3.8 (sample 3), −1.6 (sample 4), and −2.1 (sample 5)] appear to be sensitive to sample strain, with the largest (0.8) associated with the initial sample, and the smallest with the unannealed HIP sample (−8.5). A rather normal[55,56] $\Gamma^{lin} = -3(1)$ probably is appropriate. If tunneling were to make a significant contribution to α, these values of Γ would be expected to have a much greater magnitude.

D. C_p comparisons

Table I also contains data and citations to papers and other sources of C_p data for Al-Cu-Fe. The C_p data usually are presented in the form of C_p/T vs T^2 plots, with Θ_0 and γ (columns 1 and 2) given if the data can be analyzed in terms of Eq. (1a). An upturn in these plots at low temperatures suggests an additional contribution to C_p, and Θ_0 and γ cannot be determined.

The compositions (column 4) typically are those of the melts (approximately 1200 °C) from which the initial sample ingots (often ribbons from "planar flow casting" or "melt spinning") are formed by quenching to room temperature. These initial materials are annealed at 800 °C or so to obtain

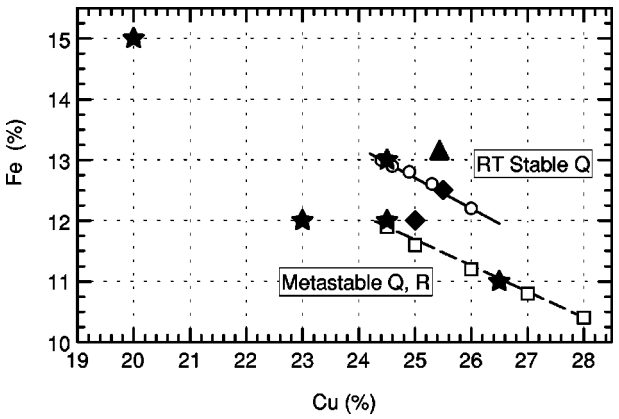

FIG. 7. ''Phase diagram'' for Al-Cu-Fe near 800 °C, from Fig. 1 in Ref. 9. (—○—) concentrations giving quasicrystals which are stable at all temperatures, (––□––) quasicrystals at 800 °C, metastable after quenching to 300 K, but rhombohedral after 600-°C anneal. (▲) present data; (♦) Lasjaunias *et al.* (Ref. 29); (⋆) Refs. 21, 25, and 57. See Table I.

the final quasicrystal samples. Figure 7, which is from Fig. 1 in Ref. 9 (see also Refs. 6–8,10, and 11), presents an approximately 800-°C phase diagram for Al-Cu-Fe for the quasicrystalline and other related phases. X-ray-diffraction spectra generally are used to determine the quality of a quasicrystal sample, and to detect secondary phases; most of the samples mentioned in Table I have been characterized in this manner.

In Fig. 7, the quasicrystalline state is stable at all temperatures on cooling to room temperature for compositions in a narrow meniscus around the upper (—○—) line. In Table I, the (24.5,13) (⋆),[25] (25.5,12.5) (♦),[29] and (25.5,13.2; nominally 25.5,12.5) (▲) present data are close to this meniscus. The pure quasicrystal which exists in a second narrow meniscus around the lower line (––□––) is metastable when quenched to room temperature, but converts to a stable rhombohedral phase when annealed near 600 °C. Thus the (24.5,12) (⋆),[21] and (26.5,11) (⋆),[25] data are for both the quasicrystalline and rhombohedral phases. The (20,15) (⋆) (Ref. 57) material has been described as a quasicrystal when quenched which downgrades when a second, Al_3Fe-type phase, appears upon annealing.[4] The (25,12) (♦) (Ref. 29) material is close to the lower meniscus, while the (23,12) (⋆) (Ref. 57) material is definitely outside either of the menisci. The actual phase diagram of Al-Cu-Fe is more complex than the above suggests;[10,11] these complexities have been ignored for present purposes.

The data for the first three ''external'' citations in Table I (associated with Klein,[20,24,29] Wang,[30,31] and their collaborators) are puzzling, with standard characterizations and ''reasonable'' γ's but very large (small Θ_0) Debye-like lattice contributions. They are anomalous for reasons which are not apparent.

The agreement between the parameters and shapes (1–4.5 K) for quasicrystal *i*- and rhombohedral *r*- (26.5,11) (Ref. 25) samples (see Fig. 2, Ref. 25) suggests an interesting similarity in the lattice properties. To further investigate this similarity, Fig. 8(a) gives a C_p/T vs T^2 plot of various C_p

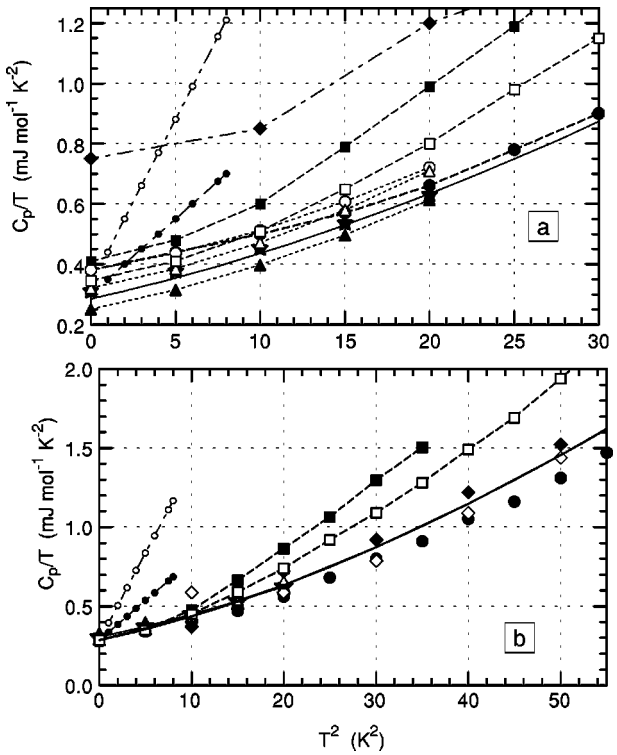

FIG. 8. A comparison of various C_p data for AlCuFe quasicrystals. (a) gives the actual data, (b) the data as normalized by adjusting the individual γ's (γ_{norm}, Table I). (—) represents the present smooth relation for the present sample 3 *i*-(25,12); (■) *i*-(25.5,12.5), (□) *i*-(25,12)-(b), Ref. 29; (△) quasicrystal, (▲) rhombohedral (26.5,11), (○) *i*-(24.5,13), Ref. 25; (⋆) *i*-(24.5,12), Refs. 25, and 21; (●) *i*-(23,12), (◇) as spun, (♦) annealed *i*-(20,15), Ref. 57; small (○) and (●), phason rich and annealed *i*-(25.5,12.5), Refs. 30 and 31. Not all symbols will appear in Figs. 8(b) and 9 because of overlapping by other symbols.

data which are cited in Table I, including only sample 3 (—-) from the present data as a reference, and excluding the off-scale as-spun *i*-(20,15) data.[57] Many of these data were read from single column journal plots, so the representations are only approximate, and conclusions drawn from them are qualitative; the lines connecting markers are for visual assistance only.

The data in Fig. 8(a) have been normalized in Figs. 8(b) and 9 by adjusting the value of γ (resulting in the γ_{norm} in column 3 Table I) until the data were (visually) superimposed symmetrically on the sample 3 (—-) curve. The three figures cover maximum temperatures to 7, 10, and 16 K, with the 16–40 K (25,12)—(b) data of Lasjaunias *et al.*[29] given in the $\Theta(T)$ plot of Fig. 5. The superposition is not perfect; slightly different shapes are apparent in Fig. 2 of Pierce *et al.*[25] The qualitative agreement, however, is surprising, since the correlations include quasicrystals and rhombohedral approximants of the same (26.5,11) composition,[25] ''as spun'' and annealed *i*-(20,15) to 16 K,[57] and the present data at various stages.

The agreement to 10 K in Figs. 8(b) and 9 between the present (12.4,13.2) sample 3 smooth relation and the as spun (◇) and annealed (♦) (20,15) data[57] is interesting, and

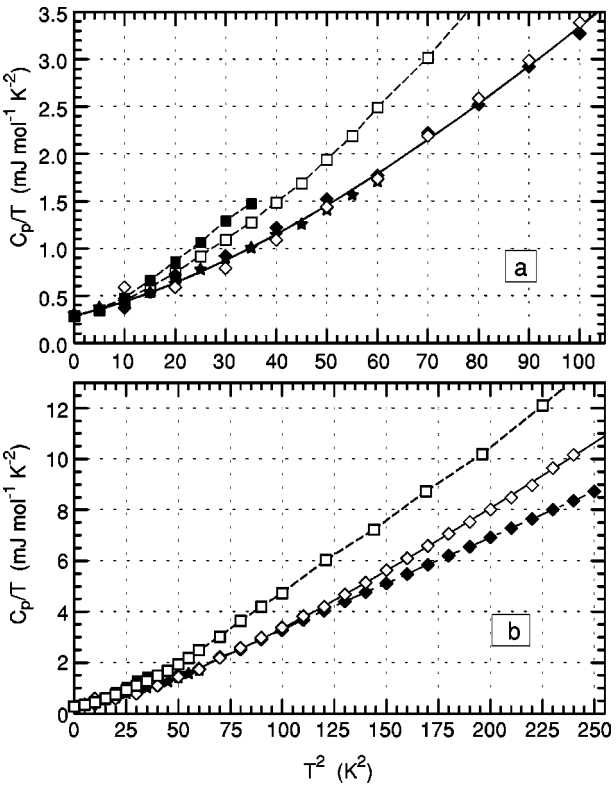

FIG. 9. As in Fig. 8(b), with extended temperature ranges.

continues for the as spun data to 16 K, while the annealed data deviate systematically to lower values with increasing temperature, presumably because of the effects of the second phase. The quenched-in strain undoubtedly contributes to the large γ_{norm} (2.12, Table I) and an upturn in C_p/T which is barely apparent in Fig. 8(b). This correspondence between the very different present sample and both the as spun and annealed samples suggests that the low-temperature lattice properties are insensitive to the state of the sample.

The (25.5,12.5) and (25,12) C_p data given by Lasjaunias *et al.*[29] show greater dispersion effects than those for the correlations. Their 0.07–6 K (25.5,12.5) data [Figs. 8(b) and 9(a)] also exhibit an upturn in C_p/T below 1 K (not apparent in Fig. 7). The composition of this sample is comparable with that of the present samples. The low-temperature (25,12)-(b) C_p data (from 0.07 to 7 K and 4 to 40 K, using different techniques)[29] are consistent with Eq. (1a), with parameters given in Table I. They show dispersion effects (Fig. 5) which are comparable to or greater than those for the present samples, and magnitudes of C_p which are increasingly larger than the present at all temperatures [Figs. 5, 8(b), and 9(a)].

IV. SUMMARY AND CONCLUSIONS

The present data are in agreement with conclusions from similar C_p data for Al-Pd-Mn that inconsistencies between C_p and inelastic neutron-scattering results are related to an extreme dispersion (deviations from Debye behavior) in $C_p(T)$ for these materials which probably is associated with the many phonons which correspond to nonmajor symmetry directions in these materials (see Sec. I.). In Figs. 3 and 4, the (- — - —) lines represent Debye (constant Θ, Γ^{lat}) behavior, as would a constant Θ in Fig. 5. The deviations from Eq. (1a) of C_p for Al-Cu-Fe as discussed by Lasjaunias *et al.*[29] are directly related to these large dispersion effects, as are the neutron-scattering discrepancies discussed by Brand *et al.*[44] C_p data should cover a relatively large temperature range to determine the magnitudes of the higher-order parameters in Eq. (1a). This extreme dispersion does not apply to the α data in Figs. 3 and 4(b); dispersion effects, however, appear as an abnormally strong temperature dependence for the lattice Grüneisen parameter, Γ^{lat} in Fig. 6, from a relatively large $\Gamma_0 = 6.8$ (suggesting a strong volume dependence of the elastic constants) to a very normal $\Gamma_\infty = 1.69$.

The present data also show that, while the annealing of the i-$Al_{61.4}Cu_{25.4}Fe_{13.2}$ quasicrystal has significant effects on the resistivity [$\rho(T)$, Fig. 1], it has only a small effect on C_p and α except at the lowest temperatures, where γ, the electronic C_p coefficient, appears to show a similar but inverse sensitivity (Table I and Figs. 2–4). The magnitudes of both ρ and γ are related to the existence of a pseudogap in the density of states at the Fermi level,[13,15–18] so it is reasonable that the pseudogap would be more sensitive to the state of the sample than the lattice properties. The comparisons with other data in Figs. 8 and 9 also show an insensitivity of C_p^{lat} to crystal composition, structure (quasicrystal, rhombohedral) and state (quenched, annealed), and sample porosity. Contrary evidence exists in the data of Wang and his collaborators[30,31] (see Table I and Fig. 8), which show large changes in the lattice properties of Al-Cu-Fe on annealing, with little dispersion and much larger lattice C_p's. The i-(25.5,12.5) and i-(25,12) C_p data of Lasjaunias *et al.*[29] [Table I and Figs. 8(b) and 9] show considerably greater dispersion effects than the present data, for reasons which are not understood. While the correlations in Figs. 8(b) and 9 support the postulate that the present lattice C_p results represent those for i-Al-Cu-Fe, we have no basis in an absolute sense for making that postulate.

Electronic and transport properties appear to indicate qualitative differences between the compositions (i)-(25-12) and i-(25.5,12.5).[20,22,24–27] The present data are for a nominal (25.5,12.5) composition, which quantitative analysis shows actually is (25.4,13.2). $\rho(T)$ data (Fig. 1) resemble closely those published for the (25,12) composition, which are appreciably smaller than those published for (12.5,25.5). This similarity, the correlations in Figs. 8(a) and 9, and the disagreement with other (25,12) and (25.5,12.5) C_p data, are puzzling.

ACKNOWLEDGMENTS

The authors are indebted to Professor J. C. Lasjaunias and Professor S. J. Poon for correspondence and allowing the use of unpublished data, and, again, to Professor Alan Goldman for suggesting the potential importance of very low-energy phonons to explain the C_p-INS inconsistencies. This manuscript has been authored by Iowa State University of Science and Technology under Contract No. W-7405-ENG-82 with the U.S. Department of Energy.

*Electronic address: swenson@ameslab.gov
[1] D. Shectman, I. Blech, D. Gratias, and J.W. Cahn, Phys. Rev. Lett. **53**, 1951 (1984).
[2] A. P. Tsai, in *Physical Properties of Quasicrystals*, edited by Z. M. Stadnik (Springer, New York, 1999).
[3] A.P. Tsai, A. Inoue, and T. Masumoto, Jpn. J. Appl. Phys., Part 2 **26**, L1505 (1987).
[4] Y. Calvayrac, A. Quivy, M. Bessière, M. Cornier-Quicandon, and D. Gratias, J. Phys. (France) **51**, 417 (1990).
[5] The compositions of Al-Cu-Fe samples alternatively may be designated as (Cu%, Fe%); i-$Al_63Cu_25Fe_12$, for example, would be referred to as (25, 12).
[6] M. Bessère, A. Quivy, S. Lefebre, J. Devaud-Rzepski, and Y. Calvayrac, J. Phys. I **1**, 1823 (1991).
[7] F.W. Gayle, A.J. Shapiro, F.S. Biancaniello, and W.J. Boettinger, Metall. Trans. A **23A**, 2410 (1992).
[8] D. Gratias, Y. Calvayrac, J. Devau-Rzepski, J. Faudot, M. Harmelia, A. Quivy, and P.A. Bancel, J. Non-Cryst. Solids **153-154**, 482 (1993).
[9] F. Hippert, R.A. Brand, J. Pelloth, and Y. Calvayrac, J. Phys.: Condens. Matter **6**, 11 189 (1994).
[10] M. Quiquandon, A. Quivy, J. Devaud, F. Faudor, S. Lefebvret, M. Bessère, and Y. Calvayrac, J. Phys.: Condens. Matter **8**, 2487 (1996).
[11] R.A. Brand, J. Pelloth, F. Hippert, and Y. Calvayrac, J. Phys.: Condens. Matter **11**, 7523 (1999).
[12] G.A.M. Reynolds, G. Golding, A.R. Kortan, and J.M. Parsey, Phys. Rev. **41**, 1194 (1990).
[13] U. Mizutani, J. Phys.: Condens. Matter **10**, 4069 (1998).
[14] Z.M. Stadnik, D. Purdie, M. Garnier, Y. Baer, A.P. Tsai, A. Inoue, K. Edagawa, S. Takeuchi, and K.H.J. Buschow, Phys. Rev. B **55**, 10 938 (1997).
[15] T. Schaub, J. Delahaye, C. Berger, T. Grenet, H. Guyot, R. Belkhou, A. Taleb-Ibrahimi, J.J. Préjean, and Y. Calvayrac, Mater. Sci. Eng., A **294-296**, 512 (2000).
[16] T. Klein, O.G. Symko, D.N. Davydov, and A.G.M. Jansen, Phys. Rev. Lett. **74**, 3656 (1995).
[17] D.N. Davydov, D. Mayou, C. Berger, C. Gignoux, A. Neumann, A.G.M. Jansen, and P. Wyder, Phys. Rev. Lett. **77**, 3173 (1996).
[18] R. Escudero, J.C. Lasjaunias, Y. Calvayrac, and M. Boudard, J. Phys.: Condens. Matter **11**, 383 (1999).
[19] T. Klein, A. Gozlan, C. Berger, F. Cyrot-Lackmann, Y. Calvayrac, and A. Quivy, Europhys. Lett. **13**, 129 (1990).
[20] T. Klein, C. Berger, D. Mayou, and F. Cyrot-Lackmann, Phys. Rev. Lett. **66**, 2907 (1991).
[21] B.D. Biggs, Y. Li, and S.J. Poon, Phys. Rev. B **43**, 8747 (1991).
[22] T. Klein, H. Rakoto, C. Berger, G. Fourcaudot, and F. Cyrot-Lackmann, Phys. Rev. B **45**, 2046 (1992).
[23] D. Mayou, C. Berger, F. Cyrot-Lackmann, T. Klein, and P. Lanco, Phys. Rev. Lett. **70**, 3915 (1993).
[24] T. Klein, C. Berger, G. Fourcaudot, J.C. Grieco, and J.C. Lasjaunias, J. Non-Cryst. Solids **153-154**, 312 (1993).
[25] F.S. Pierce, P.A. Bancel, B.D. Biggs, Q. Guo, and S.J. Poon, Phys. Rev. B **47**, 5670 (1993).
[26] A. Bilušić, A. Somontara, J.C. Lasjaunias, J. Ivkov, and Y. Calvayrac, Mater. Sci. Eng., A **294-296**, 711 (2000).
[27] A. Smontara, J.-C. Lasjaunias, C. Paulsen, and A. Bilušić, Mater. Sci. Eng., A **294-296**, 706 (2000).
[28] J. C. Lasjaunias and Y. Calvayrac, in *Proceedings of the 5th International Conference on Quasicrystals, Avignon, France*, edited by C. Janot and R. Mosseri (World Scientific, Singapore, 1995).
[29] J.C. Lasjaunias, Y. Calvayrac, and H. Yang, J. Phys. I **7**, 959 (1997).
[30] K. Wang, C. Scheidt, P. Garoche, and Y. Calvayrac, J. Phys. I **2**, 1553 (1992).
[31] K. Wang and P. Garoche, Phys. Rev. B **55**, 250 (1997).
[32] C.A. Swenson, I.R. Fisher, N.E. Anderson, P.C. Canfield, and A. Migliori, Phys. Rev. B **65**, 184206 (2002).
[33] J.J. Vanderwal, P. Zhao, and D. Walton, Phys. Rev. B **46**, 501 (1992).
[34] T. Tanaka, Y. Mitarai, and M. Koiwa, Philos. Mag. A **73**, 1715 (1996).
[35] A. Migliori and J. L. Sarro, *Resonant Ultrasound Spectroscopy* (Wiley, New York, 1997).
[36] P.S. Spoor, J.D. Maynard, and A.R. Kortan, Phys. Rev. Lett. **75**, 3462 (1995).
[37] F. Bert, G. Bellessa, A. Quivy, and Y. Calvayrac, Phys. Rev. B **61**, 32 (2000).
[38] M. Cornier-Quiquandon, A. Quivy, S. Lefebvre, E. Elkaim, G. Heger, A. Katz, and D. Gratias, Phys. Rev. B **44**, 2071 (1991).
[39] M. Quilichini, G. Heger, B. Hennion, S. Lefebvre, and A. Quivy, J. Phys. (France) **51**, 1785 (1990).
[40] M. Quilichini, B. Hennion, G. Heger, S. Lefebvre, and A. Quivy, J. Phys. II **2**, 125 (1992).
[41] M. Quilichini, B. Hennion, and G. Heger, J. Non-Cryst. Solids **153-154**, 568 (1993).
[42] M. Quilichini and T. Janssen, Rev. Mod. Phys. **69**, 277 (1997).
[43] R.A. Brand, G. Coddens, A.I. Chumakov, A.-J. Dianoux, and Y. Calvayrac, Mater. Sci. Eng., A **294-296**, 662 (2000).
[44] R.A. Brand, A.-J. Dianoux, and Y. Calvayrac, Phys. Rev. B **62**, 8849 (2000).
[45] I.R. Fisher, M. Kramer, Z. Islam, T.A. Wiener, A. Kracher, A.R. Ross, T.A. Lograsso, A.I. Goldman, and P.C. Canfield, Mater. Sci. Eng., A **294-296**, 10 (2000).
[46] A.I. Goldman, C. Stassis, M. de Boissieu, R. Currat, C. Janot, R. Bellissent, H. Moudden, and F.W. Gayle, Phys. Rev. B **45**, 10 280 (1992).
[47] T.A. Lograsso and D.W. Delaney, J. Mater. Res. **11**, 2125 (1996).
[48] T. A. Lograsso and D. W. Delaney, in *Quasicrystals*, edited by S. Takeuchi and T. Fujiwara (World Scientific, Singapore, 1998), p. 325.
[49] T.A. Lograsso, A.R. Ross, and D.W. Delaney, in *Quasicrystals*, edited by J.-M. Dubois, P. A. Thiel, A.-P. Tsai, and K. Urban, MRS Proceedings No. 553 (Materials Research Society, Pittsburgh, 1999), p. 3.
[50] C.A. Swenson, Rev. Sci. Instrum. **70**, 2728 (1999).
[51] C. A. Swenson, in *Thermal Expansion of Solids*, edited by C. Y. Ho and R. E. Taylor, CINDAS Data Series on Material Properties Vol. **I-4** (ASM, Materials Park, OH, 1998), Chap. 8.
[52] W.A. Phillips, Rep. Prog. Phys. **50**, 1657 (1987).
[53] E. S. R. Gopal, *Specific Heats at Low Temperatures* (Plenum, New York, 1966).
[54] B_S/B_T and C_p/C_v are given by $C_p/C_v=B_S/B_T=[1+\beta^2 B_S V/C_p T]=[1+\beta\Gamma T]$, where $\beta=3\alpha$ and Γ is the Grüneisen parameter which is described in Sec. III B. This ratio is 1.0036 at 100 K (and negligible; no distinction will be made

between C_p and C_v when discussing the present data), but is significant (1.022) at 300 K.

[55] T. H. K. Barron, in *Thermal Expansion of Solids* (Ref. 51), Chap. 1.

[56] T.H.K. Barron, J.G. Collins, and G.K. White, Adv. Phys. **29**, 609 (1980).

[57] S. J. Poon (unpublished).

[58] Θ and T for the approximant each were multiplied by Θ_{03}/Θ_{0Ap} ($=536\ \mathrm{K}/455\ \mathrm{K}$) to provide a direct comparison of the shapes in Fig. 6. See the comments following Eq. (4) and in Ref. 32.